Data-Driven Retrieval of Ageostrophic Surface Currents from Satellite Geostrophy and Reanalysis Winds in a Marginal Sea

Amirhossein Barzandeh, Ilja Maljutenko, Sander Rikka, Urmas Raudsepp

Department of Marine Systems, Tallinn University of Technology, Akadeemia tee 15a, Tallinn, 12618, Estonia

✉ amirhossein.barzandeh@taltech.ee

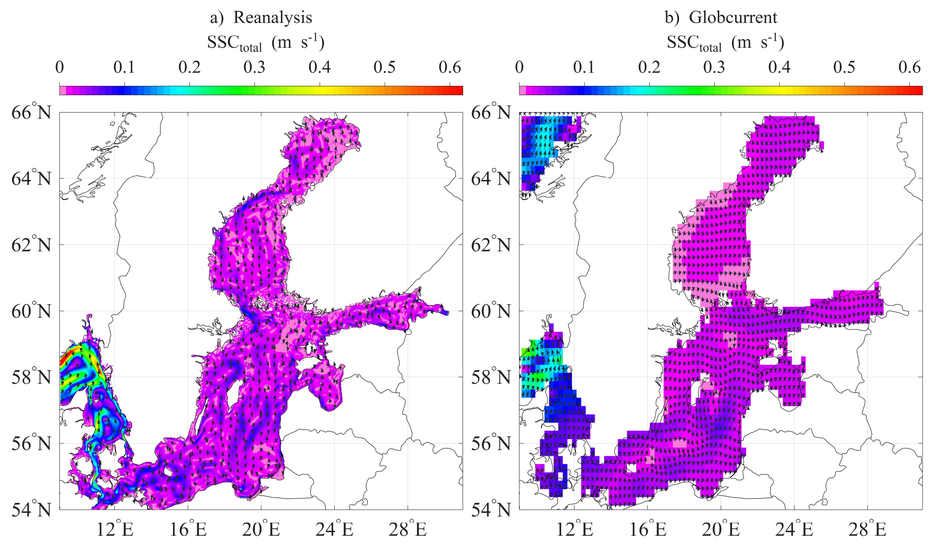

Figure 1: Mean V_{Total} for 2014–2023 from (a) the CMEMS Baltic Sea physical reanalysis based on the hydrodynamic NEMO model, and (b) the CMEMS GlobCurrent multi-platform product, where total current is represented as the sum of geostrophic and Ekman components.

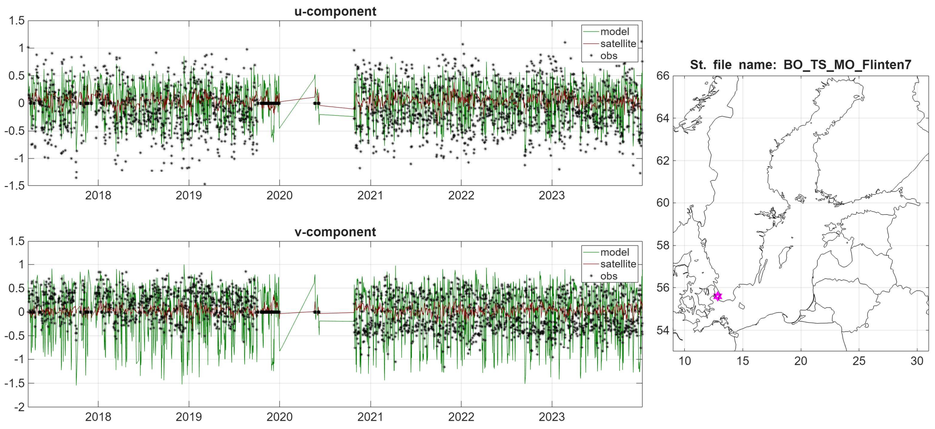

Figure 2: Comparison of V_{Total} between the CMEMS Baltic Sea physical reanalysis and the CMEMS GlobCurrent multi-platform product at an example observation station, shown for the zonal (u) and meridional (v) components.

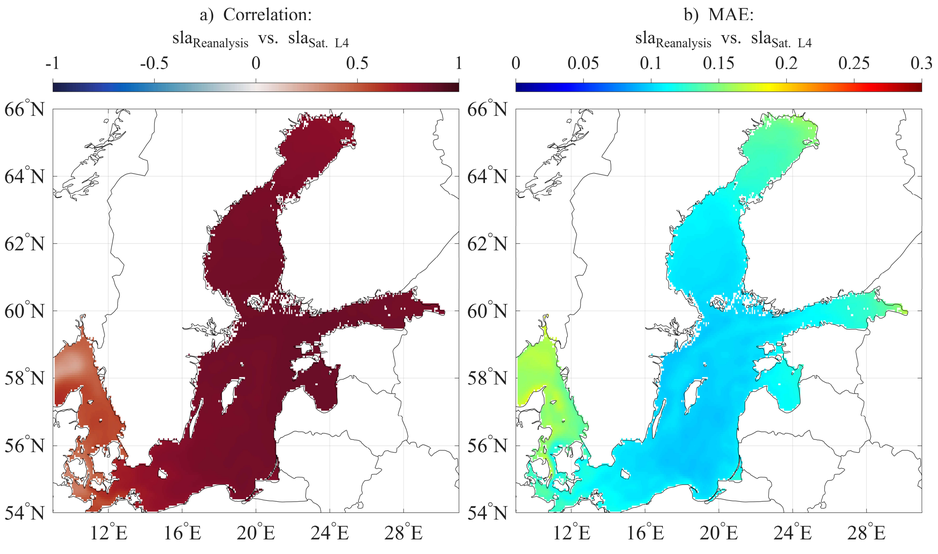

Figure 3: Agreement between CMEMS Baltic Sea reanalysis SLA and CMEMS European Seas Level-4 satellite SLA for 2014–2023. (a) Grid-point correlation between daily SLA time series. (b) Mean absolute error (MAE, m) between the same SLA fields. The high correlations (>0.75 across most of the basin) and low MAE (<0.15 m over large areas) demonstrate that the upgraded high-resolution satellite Level-4 product closely matches the reanalysis SLA. Because geostrophic currents depend on SLA gradients, this agreement indicates that both products produce consistent geostrophic current fields.

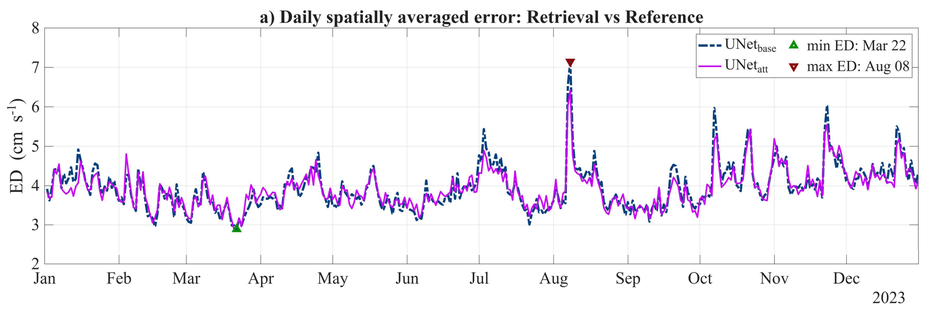

Figure 4: Performance comparison between the baseline U–Net and the fully attention-gated model for the 2023 test period. Daily spatially averaged ED between retrievals and reference V_{Ageo}.

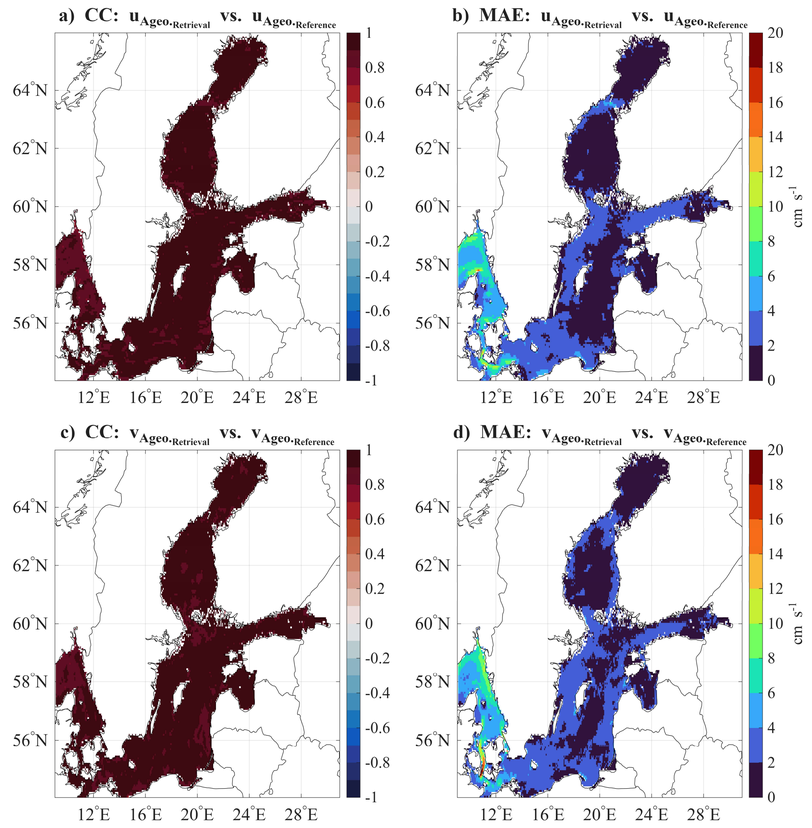

Figure 6: Basin-wide benchmarking of the attention-enhanced model over the 2023 test year. (a,c) Spatial distribution of the Pearson correlation coefficient between the model-retrieved and reference V_{Ageo} for u and v components. (b,d) Corresponding MAE fields for u and v.

Motivation

The Baltic Sea (9–31°E, 54–66°N) is a shallow, high-latitude, semi-enclosed marginal sea in which complex coastlines, strong wind forcing, stratification, and bathymetric control produce highly variable surface circulation. In this environment, daily surface flow contains both geostrophic and ageostrophic components. The geostrophic component, governed by a balance between the horizontal pressure-gradient force and the Coriolis force, can be estimated from satellite altimetry, whereas the ageostrophic component, which includes wind-driven, frictional, and other transient motions not explained by geostrophic balance, cannot be derived directly from satellite observations. In the Baltic Sea, ageostrophic processes make a substantial contribution to daily surface circulation. In many products, the unresolved ageostrophic signal is represented using simple wind-driven Ekman formulations. Yet such formulations may be inadequate in a marginal sea such as the Baltic Sea, where friction, transient adjustment, bathymetric steering, and mesoscale variability also shape daily circulation. Although full hydrodynamic models can resolve these processes more comprehensively, they are computationally expensive when the main interest is surface circulation alone, because they must evolve the full three-dimensional ocean state. We therefore adopt a data-driven approach to reconstruct the missing ageostrophic residual from satellite-derived geostrophic currents and atmospheric winds.

Methodology

Let the horizontal surface current vector be defined as $\boldsymbol{V} = (\mathbf{u}, \mathbf{v})$ and decomposed as $\boldsymbol{V_{Total}} = \boldsymbol{V_{Geo}} + \boldsymbol{V_{Ageo}}$, where $\boldsymbol{V_{Total}}$ is the total near-surface current from the hydrodynamic model $\boldsymbol{V_{Geo}}$ is the satellite-derived geostrophic current. The ageostrophic residual is therefore defined as $\boldsymbol{V_{Ageo}} = \boldsymbol{V_{Total}} - \boldsymbol{V_{Geo}}$. The learning task is to predict the daily $\boldsymbol{V_{Ageo}}$ components from the $\boldsymbol{V_{Geo}}$ components, the 10 m **wind** components, and the previous-day $\boldsymbol{V_{Ageo}}$ components, i.e.

$$\left(\boldsymbol{u_{Geo}(t), v_{Geo}(t), u_{Wind}(t), v_{Wind}(t), u_{Ageo}(t-1), v_{Ageo}(t-1)}\right) \xrightarrow[learned\ mapping]{} \left(\boldsymbol{u_{Ageo}(t), v_{Ageo}(t)}\right)$$

We used daily $\boldsymbol{V_{Geo}}$ from the Copernicus Marine Environment Monitoring Service (CMEMS) European Seas Level-4 altimetry product, $\boldsymbol{V_{Total}}$ from the CMEMS Baltic Sea physical reanalysis, and 10 m winds from the European Centre for Medium-Range Weather Forecasts Reanalysis v5 (ERA5). All fields were interpolated onto the native 0.0625° altimetry grid. A static land–sea mask was applied. Data from 2014–2022 were used for training (9 years), and 2023 was reserved for independent testing (1 year).

We developed an attention-gated convolutional U-Net (**att**) for daily $\boldsymbol{V_{Ageo}}$ component retrieval (Table 1). The model is a convolutional encoder-decoder with attention-gated skip connections, introduced to better emphasize spatially localized, dynamically active ageostrophic features. To assess the impact of attention, its performance was compared with that of a baseline U-Net without attention (base). Both models were trained end-to-end using a mean-squared error loss.

Table 1. The model consists of five encoder blocks (E1-E5), a bottleneck (B), five decoder blocks (D5-D1), and five attention gates (AG1-AG5) that modulate all skip connections. Each encoder block performs convolution (Conv), group normalization (GN), rectified linear unit activation (ReLU), and 2×2 max-pooling (MaxPool), with feature channels increasing from 16 to 512. The bottleneck applies a convolutional block with 1024 channels. Each decoder block uses transposed convolution (TConv) with stride 2, concatenation with the corresponding gated encoder features, and a Conv-GN-ReLU block. Each attention gate combines encoder and decoder features through 1×1 convolutions, ReLU, sigmoid activation, and element-wise multiplication to generate a scale-dependent gating mask. Here, H=192 and W=352 are the meridional and zonal grid dimensions, respectively; thus, H×W=192×352. The "Filters / channels" column gives the number of feature channels at each stage. The final 1×1 convolution produces the two output channels.

Stage	Block	Operation sequence	Filters / channels	Notes
Input	–	Input image	$H \times W \times 6$	$(u_{geo}, v_{geo}, \tilde{u}_{10}, \tilde{v}_{10}, u_{ageo}(t-1), v_{ageo}(t-1))$
Encoder	E1	Conv–GN–ReLU–MaxPool 2 × 2	16	Finest scale; skip gated by AG1
	E2	Conv–GN–ReLU–MaxPool 2 × 2	64	Skip gated by AG2
	E3	Conv–GN–ReLU–MaxPool 2 × 2	128	Intermediate scale; skip gated by AG3
	E4	Conv–GN–ReLU–MaxPool 2 × 2	256	Subbasin scale; skip gated by AG4
	E5	Conv–GN–ReLU–MaxPool 2 × 2	512	Deepest encoder level; skip gated by AG5
Attention	AG1	1 × 1 Conv (from D1, E1) – ReLU – 1 × 1 Conv – Sigmoid – element-wise product	4 (intermediate) / 16 (mask)	Gates E1 features using D1 context
	AG2	1 × 1 Conv (from D2, E2) – ReLU – 1 × 1 Conv – Sigmoid – element-wise product	16 (intermediate) / 64 (mask)	Gates E2 features using D2 context
	AG3	1 × 1 Conv (from D3, E3) – ReLU – 1 × 1 Conv – Sigmoid – element-wise product	32 (intermediate) / 128 (mask)	Gates E3 features using D3 context
	AG4	1 × 1 Conv (from D4, E4) – ReLU – 1 × 1 Conv – Sigmoid – element-wise product	64 (intermediate) / 256 (mask)	Gates E4 features using D4 context
	AG5	1 × 1 Conv (from D5, E5) – ReLU – 1 × 1 Conv – Sigmoid – element-wise product	128 (intermediate) / 512 (mask)	Gates E5 features using D5 context
Bottleneck	B	Conv–GN–ReLU	1024	Coarsest representation
Decoder	D5	TConv (stride 2); concat with gated E5; Conv–GN–ReLU	512	Upsample to E5 resolution
	D4	TConv; concat with gated E4; Conv–GN–ReLU	256	Upsample to E4 resolution
	D3	TConv; concat with gated E3; Conv–GN–ReLU	128	Upsample to E3 resolution
	D2	TConv; concat with gated E2; Conv–GN–ReLU	64	Upsample to E2 resolution
	D1	TConv; concat with gated E1; Conv–GN–ReLU	16	Upsample to input resolution
Output	–	Conv 1 × 1	2	$(u_{ageo}(t), v_{ageo}(t))$

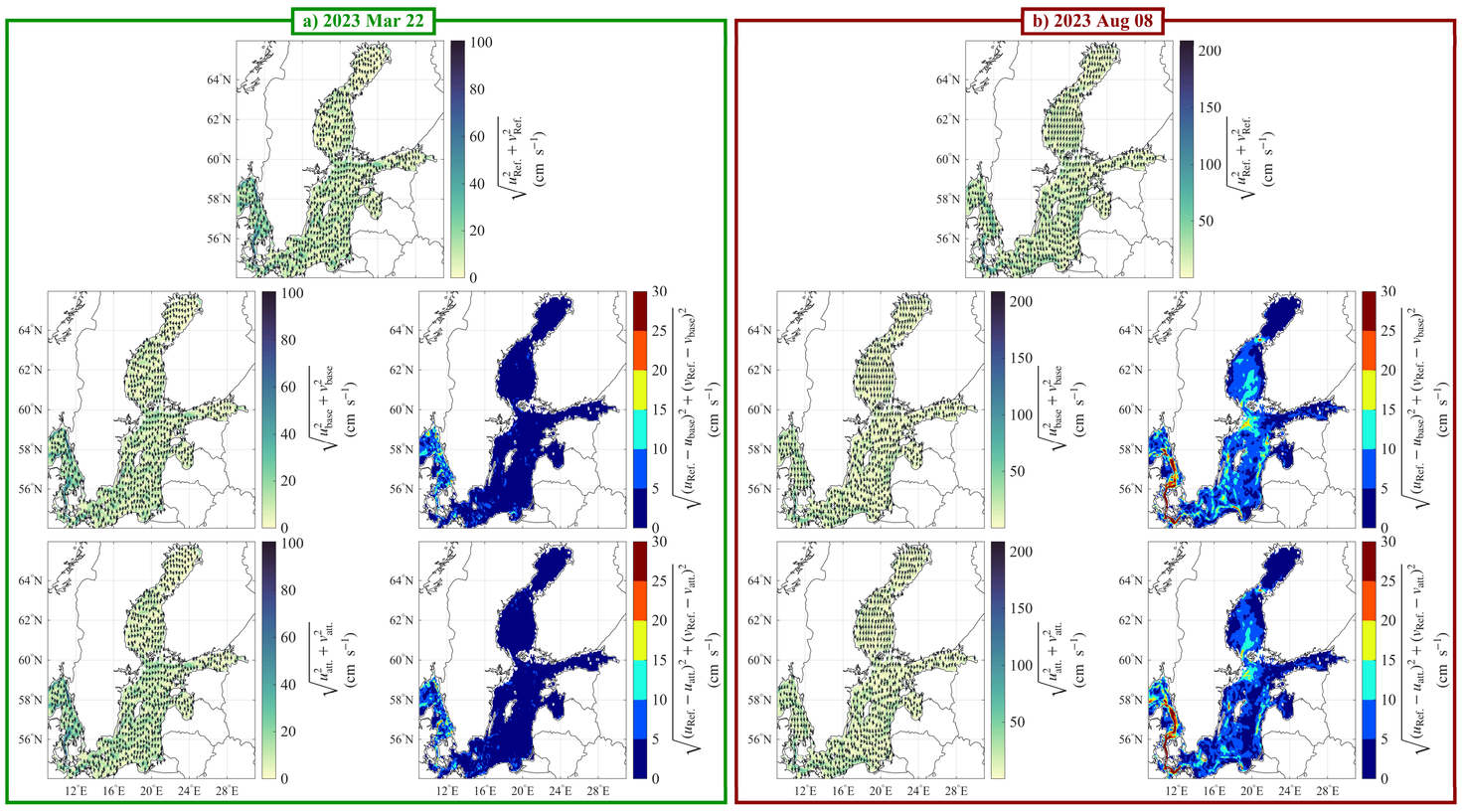

Figure 5: Reference and modeled ageostrophic surface currents for two representative dates in 2023. (a) 22 March 2023, corresponding to the day of minimum basin-averaged ED, and (b) 8 August 2023, corresponding to the day of maximum ED, as identified in Fig. 3. For each date, the panels show (top to bottom): the reference field, the UNet$_{base}$ retrieval, the UNet$_{att}$ retrieval, and the spatial ED relative to the reference for each model.

Main Findings

✓ The Baltic Sea reanalysis provides a more physically realistic representation of surface currents, resolving coastal jets, recirculations, and mesoscale structures that are strongly smoothed in satellite-based blended products such as GlobCurrent (Figs. 1 and 2). At the same time, satellite and reanalysis sea level anomalies agree well (Fig. 3), indicating that the geostrophic component is already broadly consistent between the two systems. This suggests that the weaker agreement between GlobCurrent and the NEMO-based Baltic reanalysis is mainly linked to the simplified treatment of the ageostrophic component. This supports our strategy of learning only the missing ageostrophic residual.

✓ The time series of basin-mean Euclidean distance (ED) over the independent 2023 test period shows that the ageostrophic circulation is retrieved with high skill (Fig. 4a). For most of the year, ED remains in the range of about 3–5 cm/s. The attention-gated model remains consistently below the baseline curve through most of the time series. The minimum ED occurs in late March, when the reconstructed fields closely match the reference under relatively smooth flow conditions, while the maximum ED occurs in early August during a period of stronger and more heterogeneous circulation. Even in this more difficult case, the attention model retains a smaller error peak, indicating improved robustness during dynamically active conditions.

✓ The speed and direction comparisons further support this result (Fig. 4b,c). Current direction is reproduced well, while the attention model more often yields smaller speed errors, especially for stronger currents. This shows that the main effect of attention is a consistent refinement of the magnitude and spatial localization of the reconstructed ageostrophic flow. The representative minimum- and maximum-error cases illustrate this behavior in space (Fig. 5). On the low-error day, the reconstructed field agrees closely with the reference, with weak and spatially uniform differences. On the high-error day, the circulation is much more energetic and spatially heterogeneous, with sharper gradients, narrow jets, and localized mesoscale structures. Under these conditions, the attention-gated model shows lower local errors, particularly in frontal regions, boundary currents, and other dynamically active areas. This indicates that attention improves reconstruction where the ageostrophic signal is strongest and most structured.

✓ Basin-wide benchmarking confirms that the skill is not limited to a few isolated events (Fig. 6). For both zonal and meridional ageostrophic velocity components, correlations exceed 0.9 over most of the Baltic Sea. Mean absolute errors are typically below 4–6 cm/s across most of the basin, with larger errors mainly confined to the southwestern Baltic Sea and some coastal segments. Overall, the attention-gated model delivers a modest but consistent improvement, with the clearest benefit appearing in more energetic and spatially heterogeneous cases.

✓ These results suggest that data-driven reconstruction of the ageostrophic residual could be integrated into future satellite-based sea-surface current products to improve their realism in dynamically complex marginal seas.

This study is supported by the Estonian Research Council through the AI-based Emulator for Marine Environmental Simulations (AIMES) project (project No. PSG1130)